Journal of Colloid and Interface Science 349 (2010) 354–360

Contents lists available at ScienceDirect

Journal of Colloid and Interface Science

www.elsevier.com/locate/jcis

Characterization of the wettability of thin nanostructured films in the presence of evaporation

Anita Rogacs [a,*], Julie E. Steinbrenner [a], Jeremy A. Rowlette [b], Jeffrey M. Weisse [a], Xiaolin L. Zheng [a], Kenneth E. Goodson [a]

[a] Department of Mechanical Engineering, Stanford University, 440 Escondido Mall, Bldg 530, Room 224, Stanford, CA 94305, USA
[b] Department of Electrical Engineering, Stanford University, 440 Escondido Mall, Bldg 530, Room 224, Stanford, CA 94305, USA

ARTICLE INFO

Article history:
Received 28 January 2010
Accepted 19 May 2010
Available online 23 May 2010

Keywords:
Internal contact angle
Wettability
Nanostructured wick
Evaporation
Silicon nanowire array

ABSTRACT

Vapor chambers using conventional porous membrane wicks offer limited heat transfer rates for a given thickness. This limitation can be addressed through wick nanostructuring, which promises high capillary pressures and precise control of the local porosity. This work develops a measurement technique for the wettability of nanostructured wicks based on optical imaging. Feasibility is demonstrated on a hydrophilic silicon nanowire array (SiNW) synthesized using the Vapor–Liquid–Solid (VLS) growth mechanism followed by surface plasma treatment. The wettability is determined by comparing the time-dependent liquid interface rise with a model that accounts for capillary, viscous, and gravitational forces and for evaporation. This model is demonstrated to be useful in extracting *internal* contact angle from thin (~10 μm) porous films.

1. Introduction

Aggressive reductions in the dimensions of compact electronic systems demand both low power consumption and low-profile thermal management packaging. Vapor chambers (VCs), closed two-phase, passive heat spreading devices exhibiting extremely high effective lateral thermal conductivities (>1000 W/(mK)), may provide a solution to the stringent packaging requirements. However, current VC designs are reaching their performance limit in peak heat flux capacity, owing to the limitations of conventional wicking materials and the constraints in minimizing device thickness which directly control the vertical thermal conduction resistance [1]. Conventional isotropic micro-porous wicks have fundamental limitations in their liquid delivery capacity due to the inverse relationship between permeability and capillary pressure [2]. However, it has been shown that this tradeoff can be relaxed by engineering the wick to have anisotropic structural properties which results in position-dependent permeability and pore size [3]. Although potentially very promising, this concept has yet to be applied to nano-porous films, and in particular superhydrophillic nanostructured films, where film thickness can be significantly reduced while also maintaining high permeability and total flow capacity.

The development of novel nanostructured thin film wicks requires suitable methods for extracting the effective wettability of these films. One common approach to quantifying the wettability of complex pore structures is to evaluate the apparent contact angle that exists at the moving liquid line. Variables influencing the measured contact angle are surface roughness [4], cleaning procedure [5], velocity of the contact line [6,7], thermal treatment and processing [8], among others. Hence external contact angle measurement techniques, such as goniometry [9], cannot be relied on for determining the apparent contact angle that is influenced by the internal pore variables and describes the kinetics of capillary imbibitions into the nanostructured thin film. Since the topic of this study is the evaluation of this apparent angle, herein we will refer to it as the *internal* contact angle, θ_i.

A more suitable method to determine the internal θ_i is one that involves the tracking of filling rates with time in a porous medium. When the effects of inertia, gravity and evaporation is negligible, the transient weight-tracking method combined with the simple models of Green and Ampt, and Lucas and Washburn [10–14] can accurately extract the representative internal contact angle in a porous media [15]. However, these methods lack the full capability of treating the specific issues of thin (~10 μm) nanostructured wicks where in particular the effects of evaporation cannot typically be ignored.

In this work we develop a low-cost transient imaging technique to extract the internal contact angle of thin nanostructured porous films. Although this method is applicable to a wide range of nanoporous thin films, we demonstrate the effectiveness of the technique using a thin porous film consisting of randomly oriented Si nanowire (SiNW) array.

* Corresponding author. Fax: +1 650 723 7657.
E-mail address: rogacs@stanford.edu (A. Rogacs).

0021-9797/$ - see front matter © 2010 Elsevier Inc. All rights reserved.
doi:10.1016/j.jcis.2010.05.063

Nomenclature

A, B, D	parameters defined in Table 2
C	constant defined in Table 2
d	film thickness (m)
g	gravity (m/s^2)
h	location of meniscus (m)
$\tilde{H}$	gravity-scaled non-dimensional height (–)
$\hat{H}$	evaporation-scaled non-dimensional height (–)
m	mass (kg)
$\dot{m}$	mass flux (kg/s m^2)
K	permeability (m^2)
P	pressure (Pa)
R	pore radius (m)
t	time (s)
$\tilde{T}$	gravity-scaled non-dimensional time (–)
$\hat{T}$	evaporation-scaled non-dimensional time (–)
w	width of sample (m)
W	Lambert W function

Greek symbols

μ	dynamic viscosity (kg/m s)
ν	kinematic viscosity (m^2/s)
ϕ	porosity (–)
ρ	density (kg/m^3)
σ	surface tension (N/m)
θ_i	internal contact angle (°)

Subscripts

MAX	maximum
grav	considering gravity
evap	considering evaporation
ext	extended
lv	liquid–vapor

2. Materials and methods

The intrinsic single-crystalline SiNWs were synthesized using a vapor–liquid–solid (VLS) growth method [16,17] with gold nanoparticles (40–100 nm diameter) used as a growth catalyst. Silane was used as the Si precursor along with H_2 as the carrier gas. The growth was performed at 510 °C and 20 torr for 40 min resulting in randomly oriented SiNWs (Fig. 1) with average length of 30 μm and diameter of 50 nm. It is estimated that the effective pore size of the nanowire network lies somewhere between 10 and 500 nm. Prior to wicking measurements, the SiNWs were further treated with O_2 plasma (75 W, 5 min), rendering their surfaces hydrophilic.

The experimental setup used to extract the desired film parameters is depicted in Fig. 2. A 10×30 mm^2 sample of SiNW array is vertically mounted to a micropositioning stage and then lowered into the test fluid, either n-hexane or water, at a reference time $t = 0$. A scientific-grade, externally triggered, CCD camera (Photometrics CoolSnap ES) with a sampling frequency of 5 (10) Hz and a window time of 90 (48) s captures the optical index contrast between fluid filled and dry pore regions of the sample as a function of time. Fig. 3 shows a typical sequence of recorded images. A Canny edge filter is then applied to each image in order to determine the meniscus height, h, as a function of time. The extracted curve $h(t)$ is then compared to the analytical model which accounts for the properties of both the wick and the fluid and includes as a parameter the internal contact angle, θ_i, which generally depends on the liquid type. The details of this model and its applicability will be discussed in the following section. To calibrate the method and to extract the fluid-independent pore structure parameter, $K/(R\phi)$, we use n-hexane, a low energy apolar liquid that makes approximately zero contact angle with Si and native SiO_2 [18,19]. Water was chosen as the second test liquid for its attractive thermophysical properties. In electronics cooling applications, vapor chambers are designed to operate in a low temperature range, therefore any working fluid with boiling temperature below 100 °C at the operating pressure is a good candidate. Commonly proposed working fluids are ammonia, acetone, methanol, ethanol, Freon and water; water being perhaps the most frequently used working fluid due its good heat of vaporization, surface tension and safe handling [2].

When dealing with highly volatile liquids like n-hexane, it is necessary to increase its vapor pressure in order to observe liquid rise in the thin porous film, but achieving a completely saturated environment can be challenging in practice. With this study, we demonstrate that in practical experimental conditions, characterization of thin film wettability is possible by appropriately accounting for the mass loss via evaporation. To ensure that the evaporation rate is constant during the duration of the experiment, we empirically derive the time necessary to reach quasi-static

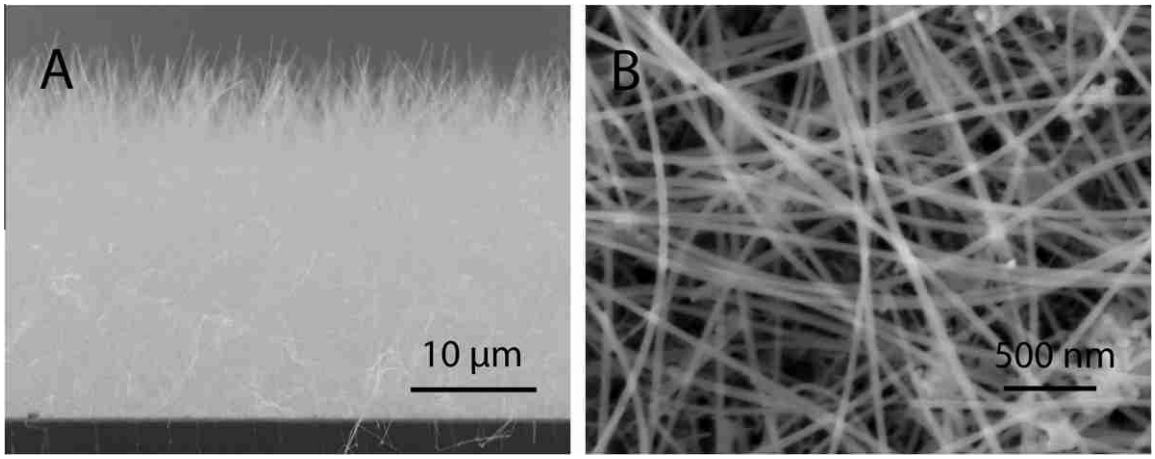

Fig. 1. Scanning Electron Microscope (SEM) images of the VLS grown SiNW sample. (A) Side-profile image of the randomly oriented nanowires supported by Si substrate. (B) Internal pore structure of the nanowire network.

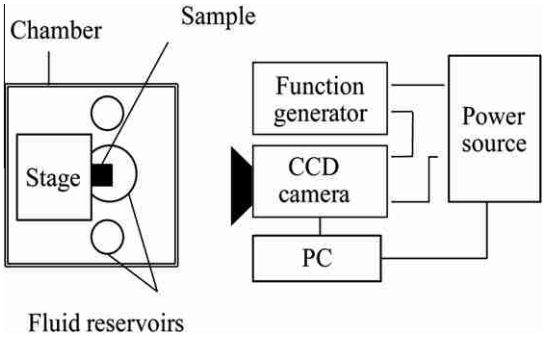

Fig. 2. Experimental setup of optical meniscus rise imaging. The three open reservoirs of the test liquid, represented as circular objects, were placed within the optically transparent chamber. Two of the reservoirs were placed away from the sample to facilitate vapor pressure increase in the chamber and the third was placed beneath the sample also serving as the liquid source for the wicking measurements.

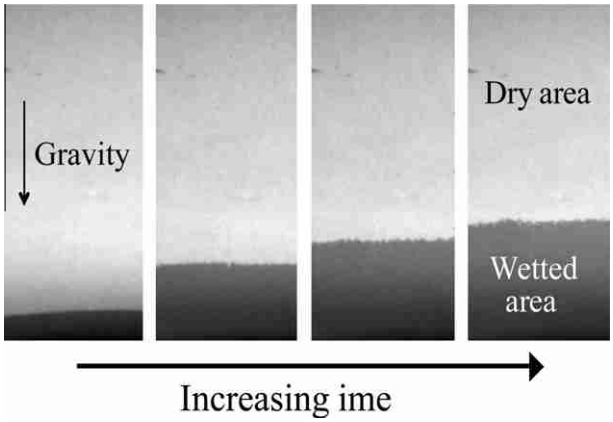

Fig. 3. Example of an image sequence acquired by CoolSnap. For visual purposes, the time between the images shown is longer (5 s) than the time between the images captured by the camera (0.1 s).

vapor pressure in the partially sealed chamber. This is accomplished by monitoring the evaporation dependence of the $h(t)$ curve as a function of the elapsed time. It was observed that in the case of *n*-hexane and water, waiting longer than 4 days and 2 h, respectively, had no quantifiable effect on the $h(t)$ curve. Therefore, after the above specified time periods and for the duration of our experiments (~100 s) we assumed steady state vapor pressure condition.

When working with nanostructured thin films with effective pore size in the order of 100 nm or less, water pH variation due to silanol group deprotonation may occur during the measurement. To stabilize this pH fluctuation, water was buffered with 20 mM acetic acid and titrated with sodium hydroxide to a pH of 4.7 at a temperature of 19.4 °C. The test liquids used in the experiments (HPLC grade *n*-hexane and DI water) were obtained from Fisher Scientific, Gibco and Sigma, respectively. The properties of the test fluids listed in Table 1 were obtained from NIST Standard Reference Database #69 at the temperature measured during the experiments ($T = 20 \pm 0.5$ °C).

3. Data analysis and parameter extraction

In this section, we consider the physically appropriate model for predicting the meniscus height vs. time, from which we extract the internal contact angle for a given fluid. Fig. 4 depicts the sample geometry for the problem to be solved. We apply momentum and mass balance on the superficial (volume averaged) flow while

Table 1
Fluid properties at $T = 20$ °C.

Sample fluids	σ_{lv} (mN m^{-1})	ρ (kg m^{-3})	μ (mPa s)
n-hexane	18.5	659	0.31
Water	72.1	998	1.0

making the following assumptions: (a) the fluid is incompressible, (b) the friction effect of displaced air and the entry effects in the liquid reservoir are negligible, (c) the film thickness is significantly smaller than the width of the sample ($d \ll w$) and (d) the evaporation rate is temporally and spatially constant. Furthermore, given the relatively long timescales of the measurements, inertial effects are deemed to be negligible and are therefore dropped from the analysis [20]. We arrive at a general describing function (1) of the porous nanowick system, which we note includes capillary, viscous, gravity and evaporation effects [21].

$$\frac{dh}{dt} = \frac{2K\sigma_{lv}\cos\theta_i}{R\mu\phi}\frac{1}{h} - \frac{\dot{m}_{evp}}{2d\rho\phi}h - \frac{g\rho K}{\mu\phi} \tag{1}$$

Eq. (1) can be solved analytically [21], and it would seem that the full solution would be appropriate for extracting the desired parameters. However, we find that the general solution introduces ambiguity in the extraction of certain wicking properties under common experimental conditions and therefore should be simplified further. For example, when the hydrostatic pressure of the liquid column is weak relative to the capillary pressure at the meniscus, it becomes impractical to extract meaningful values of R, ϕ/K, θ_i and the evaporation rate, $\dot{m}_{evp}$ [kg/m^{2}s]. For immediate reference, we have tabulated the full solution of (1) along with its various limiting forms in Table 2 for the cases of varying relative importance of evaporation and gravitational effects. The derivation of *Models 1*, *2*, and *4* can be found in the references listed in Table 2. To derive *Model 3*, we neglect the gravity term which reduces Eq. (1) to

$$\frac{dh}{dt} = A\frac{1}{h} + Bh \tag{2}$$

where A and B are listed in Table 2.

With the substitution $\varphi(t) = h^2$, Eq. (2) reduces to a linear, first order, inhomogeneous ordinary differential equation:

$$\frac{d\varphi}{dt} = 2A + 2B\varphi \tag{3}$$

which, after multiplying by the integration factor, $\exp(-\int 2Bdt)$, and integrating over the time, can be solved explicitly for $\varphi(t)$. Rewriting the resulting equation in terms of $h = \sqrt{\varphi}$ provides the explicit solution for the liquid height as a function of time.

$$h = \sqrt{\frac{A}{B}(e^{2Bt} - 1)} \tag{4}$$

Also listed in Table 2 is the steady state ($t \to \infty$) height of the meniscus, which approaches a finite value if either the hydrostatic pressure balances the capillary pressure [22], the mass loss via evaporation balances the incoming flow [21], or, as in case of the most comprehensive model, a combination of the two effects halts the advancement of the liquid front [21].

3.1. Selection of appropriate theoretical model for nanostructured films

The effective internal contact angle can be obtained by fitting the measured meniscus height data as a function of time to the appropriate limiting form in Table 2. *Model 4* is the most comprehensive of the four models as it includes contributions from both

Table 2
Four limiting solutions of liquid rise in porous media.

Models	*Rise/time relationship*	*Maximum height*
1. Negligible gravitational and evaporation effects [10,13]	$h(t)=\sqrt{2At}$	$h_{MAX}=\infty$
2 . Negligible evaporation effects [22,23]	$h(t)=-\frac{A}{D}\left[1+W\left(-\exp\left(-1-\frac{D^2t}{A}\right)\right)\right]$	$h_{MAX\_grav}=\frac{-A}{D}$
3. Negligible gravitational effects	$h(t)=\sqrt{\frac{A}{B}\exp(2Bt)-\frac{A}{B}}$	$h_{MAX\_evp}=\sqrt{\frac{-A}{B}}$
4. Full, implicit solution to Eq. (1) [21]	$t=\frac{1}{2B}\left(\ln\left\lvert\frac{Bh^2+Dh+A}{A}\right\rvert\right)-\frac{D}{2B\sqrt{D^2-4BA}}\times\left(\ln\left\lvert\frac{\left(2Bh+D-\sqrt{D^2-4BA}\right)\left(D-\sqrt{D^2-4BA}\right)}{\left(2Bh+D+\sqrt{D^2-4BA}\right)\left(D+\sqrt{D^2-4BA}\right)}\right\rvert\right)$ where $A=\frac{2K\sigma_{lv}\cos\theta_i}{R\mu\phi}$; $B=\frac{-C_{evp}}{2}=\frac{-\dot{m}_{evp}}{2d\rho\phi}$; $D=\frac{-g\rho K}{\mu\phi}$	$h_{MAX\_evap\_grav}=\frac{-D}{2B}+\sqrt{\left(\frac{D}{2B}\right)^2-\frac{A}{B}}$

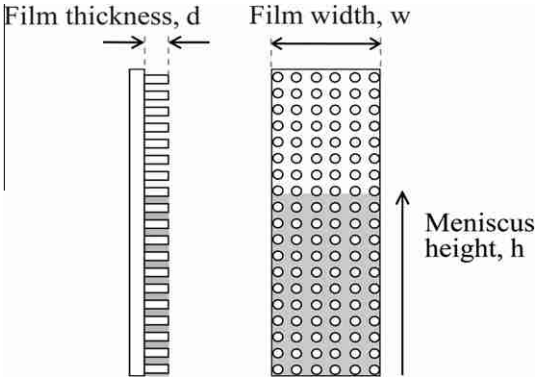

Fig. 4. SiNW sample geometry. Nanowire film thickness is *d*, width of sample is *w*, and the location of the liquid vapor interface measured from the bottom of the sample at time *t* is *h*.

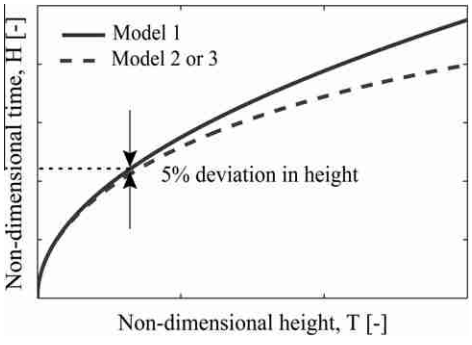

Fig. 5. Location of 5% deviation of *Model 1*, which neglects both gravity and evaporation from the extended (*Model 2*: for gravity and *Model 3*: for evaporation) solutions.

capillary and viscous forces, as well as gravity and evaporation. Hence, its use in extracting material properties has great appeal. When R, and ϕ/K are known a priori, *Model 4* returns both the contact angle, θ_i, and the evaporation constant, C_{evp}, accurately. However, in the case of unknown structural constants and under common experimental conditions, this extended model can fail to fit for the unknown parameters, unless the capillary pressure term, $2\sigma_{lv}\cos\theta_i/R$, and the hydrostatic pressure term, $g\rho h$, are of the same order of magnitude. When this condition is met, it is crucial to select the appropriate simplified model for analysis. In the following two sections we will present guidelines for selecting the appropriate model for analysis by examining the contributions of gravity and evaporation on the filling rate independently. We will show that gravity has negligible influence on the liquid uptake velocity in thin nanostructured films and therefore either *Model 1 or 3* should be used for data analysis depending on the relative importance of evaporation effects.

3.2. Flow regime with negligible gravitational effects

Although very few of the film parameters may be known a priori, we can arrive at a conservative estimate for the sample size below which gravitational effects can safely be ignored. Shown in Fig. 5, we define a non-dimensional time [22], $\tilde{T}=tD^2/A$, at which the gravity extended model [23], *Model 2*, deviates by a certain percentage from *Model 1*, which neglects both gravitational and evaporation effects. A non-dimensional height can then be defined as $\tilde{H}=h_{\mathrm{grav}}(\tilde{T})/h_{\mathrm{MAX\_grav}}=1+W(-e^{-1-\tilde{T}})$, where $W(\tilde{T})$ represents the Lambert W function [22], which is the inverse function of $x=W(x)e^{W(x)}$, where e is the natural exponential function. The non-dimensional times and heights associated with 1%, 5% and 10% deviation from *Model 1* have been evaluated in [22] and are reported here for reference in Table 3.

Combining the expression for $h_{\mathrm{MAX\_grav}}$, listed in Table 2, with the non-dimensional height listed based on a 5% deviation error, we arrive to the condition, $R\cdot h_{\mathrm{grav}}\leqslant 0.8\times10^{-6}$, which guarantees that the dynamics of *n*-hexane imbibition will not be measurably influenced by gravity. When the effective pore size of the film is unknown, the film thickness, d, may be used as a conservative estimate for the pore radius. For example, in the case of *n*-hexane, wicking into a porous film with thickness of 10 μm, gravity can be neglected up to 8 cm rise or over 3 in., far greater than a typical sample size. In the case of water, even if the solid is poorly hydrophilic (e.g. $\theta=80°$), the regime with negligible gravitational effects only decreases by a factor of 2. Therefore, we can safely conclude that gravitational effects can be ignored for thin ($\leqslant$10 μm) film samples with typical ($\leqslant$4 cm) specimen heights. Hence, either *Model 1 or 3* will be suitable for data processing and parameter extraction. For specimens with dimensions larger than the above recommendations, gravity will gain in importance and *Model 2 or*

Table 3
Valid height range of *Model 1* considering gravity only (*Model 2*) [27].

Error (%)	$\tilde{H}=\frac{h_{\mathrm{grav}}}{h_{\mathrm{MAX\_grav}}}$	$\tilde{T}=\frac{D^2t}{A}$
1	29.8×10^{-3}	4.52×10^{-4}
5	144×10^{-3}	115×10^{-4}
10	277×10^{-3}	475×10^{-4}

4 should be used. It remains to be determined whether or not evaporation effects can be neglected.

3.3. Flow regime with negligible evaporation effects

Unlike the case for gravity, it is difficult to determine the influence of evaporation without the knowledge of the parameters of interest ($K/(R\phi)$, θ_i, C_{evp}). Thankfully, the inclusion of the evaporation term in *Model 3* has no adverse effect on the extraction of the fluid-independent parameter, $K/(R\phi)$, and *internal* contact angle, θ_i, therefore it is the authors recommendation to use *Model 3* for all porous thin films. While *Model 3* remains suitable for any evaporation condition, one may still be interested in determining an estimate for the sample size below which evaporation effects can safely be ignored. In order to determine the limit on sample size, we identify the range of validity of *Model 1* in comparison to *Model 3*, which includes evaporation effects but which neglects the effects of gravity. The height at which the evaporation extended model deviates 5% from *Model 1* can be found by solving:

$$(100\% - 5\%)h_1 = h_3 \tag{5}$$

where the subscript refers to the model number. Substituting the expression for h_1 and h_3 from Table 2 and canceling out common terms yields

$$0.95^2 C_{evp} t = 1 - e^{-C_{evp} t} \tag{6}$$

Non-dimensionalizing time gives:

$$t = \frac{\hat{T}}{C_{evp}} \tag{7}$$

and Eq. (7) simplifies to

$$0.95^2 \hat{T} = 1 - e^{-\hat{T}} \tag{8}$$

Solving Eq. (8) numerically gives $\hat{T} = 0.209$. Then substituting $\hat{T}$ into the non-dimensional height, we get

$$\hat{H} = \frac{h_{evp}(\hat{T})}{h_{MAX\_evp}} = \sqrt{(1 - e^{-\hat{T}})} = 0.434 \tag{9}$$

$\hat{H}$, the conditions for when *Model 1* is valid are reported in Table 4.

Since it was determined that gravitational effects can be neglected in thin films ($d \sim 10\ \mu m$), the liquid front reaches a finite value only if the mass loss via evaporation balances the incoming flow. If this occurs during the sample duration, the maximum measured height, h_{MAX_evp}, and the chosen percentage deviation error in Table 4 provides the estimate for the sample size, h_{evp}, below which evaporation effects can be ignored. If the liquid front does not halt during the experiment, *Model 3*, can still be safely used to evaluate the fluid-independent parameter, $K/(R\phi)$, and the fluid-specific evaporation constant, C_{evp}, which in turn, allows the evaluation of h_{MAX_evp} using the expressions found in Table 2.

3.4. Sensitivity analysis

To understand the capability and the limitation of the characterization technique, we will quantify the relative importance of the parameters of interest in *Model 3*, via a sensitivity analysis.

Table 4
Valid height range of *Model 1* considering evaporation only (*Model 3*).

Error (%)	$\hat{H} = \frac{h_{evp}}{h_{MAX\_evp}}$	$\hat{T} = C_{evp} t$
1	199×10^{-3}	40.3×10^{-3}
5	434×10^{-3}	209×10^{-3}
10	595×10^{-3}	437×10^{-3}

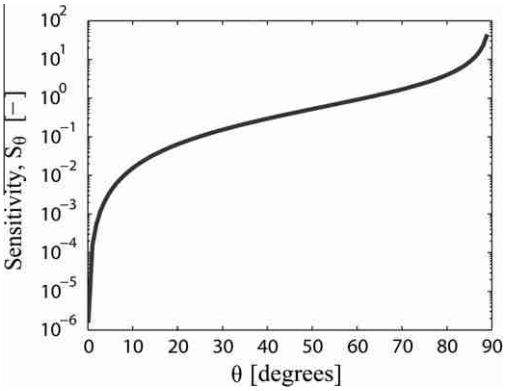

Fig. 6. Sensitivity of liquid height with respect to the *internal* contact angle between liquid and pore surface.

Among different approaches to calculate sensitivity, in this work we use logarithmic sensitivity (%/%) of the liquid height with respect to contact angle, Eq. (10a), evaporation constant, Eq. (10b), and fluid-independent film parameter, Eq. (10c).

$$|S_\theta| = \frac{d(\log h)}{d(\log \theta_i)} = \frac{\theta_i \tan \theta_i}{2} \tag{10a}$$

$$|S_C| = \frac{d(\log h)}{d(\log C_{evp})} = \frac{1}{2}\left(1 + \frac{C_{evp} t e^{-C_{evp} t}}{e^{-C_{evp} t} - 1}\right) \tag{10b}$$

$$|S_{LP}| = \frac{d(\log h)}{d(\log(K/R\phi))} = \frac{1}{2} \tag{10c}$$

Shown in Fig. 6, the absolute magnitude of logarithmic sensitivity of the liquid height with respect to θ_i increases monotonically with increasing contact angle but is independent of time. Hence, sensitivity associated with contact angles below 10° is sufficiently weak to make extraction of the angle impractical, regardless of the measurement duration, when one considers that typical uncertainties (spatial and temporal) associated with this experimental technique is in the order of 10^{-2}. On the other hand, the logarithmic sensitivity of the liquid height with respect to C_{evp} is a strong function of both time and the magnitude of the evaporation. If the non-dimensional time, $\hat{T} = C_{evp} t$, is chosen as the independent variable, the sensitivity function, $S_{Cevp}(t, C_{evp})$, a two-dimensional surface, collapses to a single curve as shown in Fig. 7. Intuitively, as the evaporation rate increases, the sensitivity to that parameter is enhanced. Furthermore, for a given evaporation constant, the sensitivity to C_{evp} increases with time but saturates at a value of 1/2 for values of $\hat{T} > 5$. It is apparent that no significant gain in sensitivity is obtained for times longer than $\sim 5/C_{evp}$. Lastly, we find that the sensitivity of *Model 3* to the fluid-independent film parameter, $K/(R\phi)$, is independent of time as well as its own magnitude; hence, sample and mea-

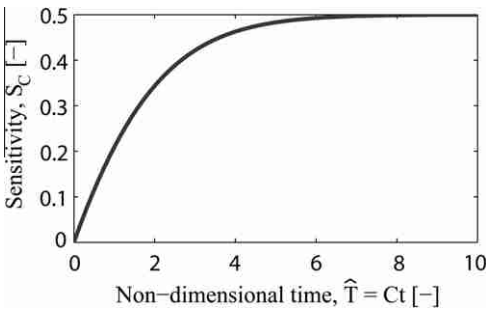

Fig. 7. Sensitivity of liquid height with respect to the evaporation constant, $C_{evp} = \dot{m}_{evp}/(\rho\phi d)$ of the test liquid.

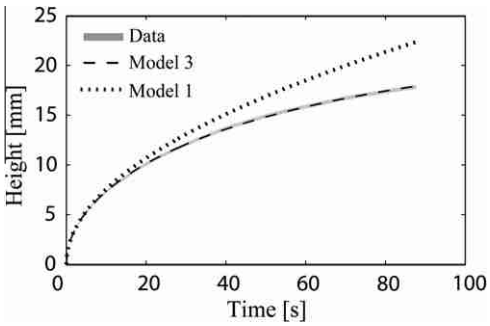

Fig. 8. Water data curve-fitted with the evaporation extended model (*Model 3*). The shaded gray region and the black dashed line represent the data collected with uncertainty and the fitted solution respectively. Using the extracted parameters from Table 5, *Model 1* is plotted for comparison. (For interpretation of the references to colour in this figure legend, the reader is referred to the web version of this article.)

Table 5
Results of parameter extraction from *n*-hexane and water data using the evaporation extended model (*Model 3*).

Fluid	Structural constant, $K/\phi R$ ($\times 10^{-8}$ m)	Internal contact angle, θ_i (°)	Evaporation constant, C_{evp} ($\times 10^{-3}$ s^{-1})
n-hexane	2.36 ± 0.06	0	2.0 ± 0.2
DI water	2.36 ± 0.06	30 ± 3	11.5 ± 0.8

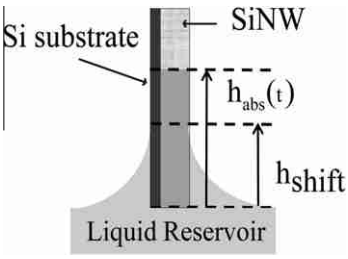

Fig. 9. Externally suspended liquid on the surface of a Si nanowire film. If the outer surface of the nanowire array is not sealed or treated to acquire hydrophobic properties, liquid is delivered into the array from the side surface in addition to the bottom edge of the sample, as modeled. By default, the meniscus height, $h_{abs}(t)$ is measured with respect to the bottom of the substrate. Immediately upon contact with the fluid, external flow rises on the side of the sample up to height, h_{shift}. In this work, this spatial uncertainty was addressed through optimization of h_{shift}, as an additional parameter in *Model 3*. All returned values for the h_{shift}, were consistent with the location approximated by visual inspection.

surement characteristics have no effect on the ease of extraction of this parameter.

4. Results and discussion

The characterization technique described in previous sections is applied to the VLS grown SiNW array using the evaporation extended model, *Model 3*, and the results are shown in Fig. 8. In Table 5, we list the extracted parameters from the two sets of measurements performed using *n*-hexane and water. Based on four independent measurements of *n*-hexane, the *n*-hexane specific evaporation constant, $C_{evp\_n\text{-hexane}}$ and the fluid-independent parameter of the SiNW array, $K/(R\phi)$ were extracted making use of the assumed 0° contact angle. Finally, the water specific *internal* contact angle, θ_i, and evaporation constant, C_{evp_water}, were extracted from two independent measurements of buffered DI water. The sources of the uncertainty in the final values of the extracted parameters include errors associated with the spatial and temporal resolution of the CCD camera and the spatial uncertainty introduced by the externally suspended liquid shown in Fig. 9.

To the best of our knowledge, we are the first to report on the value of the water specific *internal* contact angle in SiNW array. Due to the lack of wettability data on these types of structures, we can only state that the resulting *internal* contact angle, 30°, lies within the range of reported values for *external* contact angle (10–45°) for Si wafers with and without an oxide layer [5,8,24–28]. The relatively large range for these reported values are a result of variations in surface roughness [29], cleaning procedure [27], pH [30], thermal treatments and SiO_2 growth conditions [8].

Fig. 8, we also presented the solution of *Model 1* for the water meniscus height rise with the fluid-independent film parameter and *internal* contact angle. The large deviation between the two models clearly proves that neglecting evaporation in wettability characterization of porous thin films can lead to significant error. To quantify the height of liquid penetration above which the lack of the evaporation term in the analytical model would adversely affect the extracted parameters, we evaluated h_{evp} using formula for the 5% deviation in error from Table 5. Given the values for C_{evp}, $K/(R\phi)$ and θ_i in Table 5, we found that in this study, *Model 1* would only be suitable for analysis of liquid height rise of up to 9.77 mm.

5. Conclusion

The presence of evaporation often plagues wettability characterization attempts, as independent determination of its influence on the fluid-wick system can be challenging. In this work, we showed that for thin (~10 μm) porous films, the extraction of *internal* contact angle, θ_i, and the fluid-independent film parameter $K/(R\phi)$, in the presence of evaporation is achievable using a low-cost, non-contact, optical tracking methodology. In the fluid tracking methodology, an analytic model which incorporates the effects of evaporation was used to extract the fluid-independent parameter of a VLS grown SiNW array. We are able to extract with high confidence, the *n*-hexane and water specific evaporation constants as well as the water specific *internal* contact angle, the first to be reported on such films. Furthermore, we present guidelines for determining the maximum thin film sample size for a specific set of experimental conditions that would effectively ensure negligible influence of gravity or evaporation. For typical thin film sample sizes and experimental conditions, we have concluded that the influence of gravitational force is negligible, but evaporation plays a significant role in establishing filling rate. It is therefore our recommendation to use *Model 3* (Table 2) for wettability characterization for typical nanostructured porous thin films. To offer understanding of the capability and limitation of this characterization technique, we quantified the relative importance of the extracted parameters via a sensitivity analysis.

Acknowledgments

The authors are grateful for the support of this work by National Science Foundation and Toyota R&D Co. Ltd.

References

[1] R.S. Prasher, J. Electron. Packag. 125 (2003) 378.
[2] A. Faghri, Heat Pipe Science and Technology, Taylor & Francis, Washington, DC, 1995.
[3] X. Huang, G. Franchi, J. Porous Mat. 15 (2008) 635.
[4] R. Wenzel, Ind. Eng. Chem. 28 (1936).
[5] L. Klintberg et al., Sens. Actuators, A 103 (2003) 307.
[6] G. Martic, J. De Coninck, T.D. Blake, J. Colloid Interface Sci. 263 (2003) 213.
[7] B. Lavi, A. Marmur, J. Bachmann, Langmuir 24 (2008) 1918.
[8] R.R. Thomas et al., J. Electrochem. Soc. 143 (1996) 643.

[9] A. Neumann, R. Good, Surf. Colloid Sci. 11 (1979) 47.
[10] W. Green, G. Ampt, J. Agric. Sci. 4 (1911) 1.
[11] J. Schoelkopf et al., Colloids Surf., A 206 (2002) 445.
[12] R. Lucas, Kolloid-Zeitschrift 23 (1918) 15.
[13] E.W. Washburn, Phys. Rev. 17 (1921) 273.
[14] A. Siebold et al., J. Colloid Interface Sci. 186 (1997) 60.
[15] V. Gurau et al., J. Power Sources 160 (2006) 1156.
[16] A. Morales, Science 279 (1998) 208.
[17] R.S. Wagner, W.C. Ellis, Appl. Phys. Lett. (1964).
[18] Y. Takata et al., Langmuir 22 (2006) 1715.
[19] B.M. Law et al., Langmuir 19 (2003) 8380.
[20] N. Fries, M. Dreyer, J. Colloid Interface Sci. 327 (2008) 125.
[21] N. Fries et al., J. Colloid Interface Sci. 321 (2008) 118.
[22] N. Fries, M. Dreyer, J. Colloid Interface Sci. 320 (2008) 259.
[23] D. Barry et al., J. Hydrology 142 (1993) 29.
[24] S.-J. Kim et al., J. Vac. Sci. Technol., B: Microelectron. Nanometer Struct. 26 (2008) 189.
[25] M. Harris, G. Appel, H. Ade, Macromolecules 36 (2003) 3307.
[26] R.G. Horn, D.T. Smith, W. Haller, Chem. Phys. Lett. 162 (1989) 404.
[27] C.W. Extrand, Y. Kumagai, J. Colloid Interface Sci. 191 (1997) 378.
[28] V. Atanasov et al., Biophys. J. 89 (2005) 1780.
[29] A.B.D. Cassie, S. Baxter, Trans. Faraday Soc. 40 (1944) 546.
[30] H. Barhoumi et al., Langmuir 26 (2010) 7165.